Editors' Suggestion | Featured in Physics

Using Optical Tweezers to Simultaneously Trap, Charge, and Measure the Charge of a Microparticle in Air

Andrea Stoellner,[1] Isaac C. D. Lenton,[1] Artem G. Volosniev,[2] James Millen,[3] Renjiro Shibuya,[4] Hisao Ishii,[4] Dmytro Rak,[1,5] Zhanybek Alpichshev,[1] Grégory David,[6] Ruth Signorell,[6] Caroline Muller,[1] and Scott Waitukaitis[1,*]

[1]*Institute of Science and Technology Austria, Am Campus 1, 3400 Klosterneuburg, Austria*
[2]*Center for Complex Quantum Systems, Department of Physics and Astronomy, Aarhus University, Ny Munkegade 120, DK-8000 Aarhus C, Denmark*
[3]*King's College London, Strand Campus, London WC2R 2LS, United Kingdom*
[4]*Chiba University, 1-33, Yayoi-cho, Inage-ku, Chiba 263-8522, Japan*
[5]*Institute of Experimental Physics, Slovak Academy of Sciences, Watsonova 47, 040 01 Košice, Slovakia*
[6]*ETH Zürich, Rämistrasse 101, 8092 Zürich, Switzerland*

(Received 24 July 2025; accepted 2 October 2025; published 20 November 2025)

Optical tweezers are widely used as a highly sensitive tool to measure forces on micron-scale particles. One such application is the measurement of the electric charge of a particle, which can be done with high precision in liquids, air, or vacuum. We experimentally investigate how the trapping laser itself can electrically charge such a particle, in our case a ∼1 μm SiO_2 sphere in air. We model the charging mechanism as a two-photon process which reproduces the experimental data with high fidelity.

DOI: 10.1103/5xd9-4tjj

Optical tweezers are exquisitely well suited for sensing forces in settings ranging from the interactions of colloidal particles [1,2] to the chemistry and morphology of microdroplets [3,4] to precise manipulation of micron-scale objects [5,6]. When applied to probe electrical forces, this remarkable sensitivity can be used to measure the charge of small objects, akin to the famous Millikan oil-drop experiment [7] with subelectron precision. This capability has been useful in a variety of areas, including studies aimed at the charging dynamics of colloidal particles in nonpolar liquids [8–11], the precise determination of particle mass [12], and the measurement of electric fields [13], among others [14–18]. Well before these recent Letters, the first experiments to measure the charge of an optically levitated particle were carried out by Ashkin and Dziedzi [19], who observed that the trapping light could also *cause* certain particles to become charged. To the best of our knowledge, however, this effect has not been explored further since.

In this Letter, we study in detail the nonlinear photoelectric charging of a submicron particle held in a high-intensity optical trap in air. We work in a dual-beam horizontal configuration with tunable laser intensity [20], allowing us to systematically study the laser's effect on the charging dynamics. Working with high-purity (> 99.9%) amorphous silica, we find charging dynamics that are indicative of a two-photon process. Based thereon, we develop a mathematical model that closely reproduces our experimental charging vs time curves. With straightforward modifications, the use of optical tweezers to simultaneously charge and measure the charge of individual microscopic objects should be applicable to a wide variety of situations, ranging from fundamental studies of electronic properties to charge dynamics in aerosol physics and cloud electrification.

The experimental setup is sketched in Fig. 1. We use a continuous wave 532 nm laser (Laser Quantum, opus 532, 3W) to trap a submicron, amorphous silica (SiO_2) sphere (Cospheric SiO2 MS-2.0, nominal radius $r \approx 0.35$ μm, density of 2.0 g/cm^3). The initially free-space beam passes through a polarizing beam splitter (PBS) for easy intensity tuning and is then divided by a second PBS into two arms of equal power. Subsequently, each arm is coupled into a single-mode optical fiber (Thorlabs, FPC021) to facilitate beam transport, polarization control, and spatial filtering. The two beams are brought back to free space and expanded to ∼0.5 cm by two collimators (Thorlabs, TC25APC-532) shortly before they enter the grounded aluminum experimental chamber held at atmospheric pressure. Two lenses (Thorlabs, A240TM-A, focal length of 8 mm) inside the chamber focus the orthogonally polarized beams to form a counterpropagating optical trap (numerical apertures 0.29, ∼6 μm separation between foci). The lens holders are machined from copper and simultaneously serve as

*Contact author: scott.waitukaitis@ista.ac.at

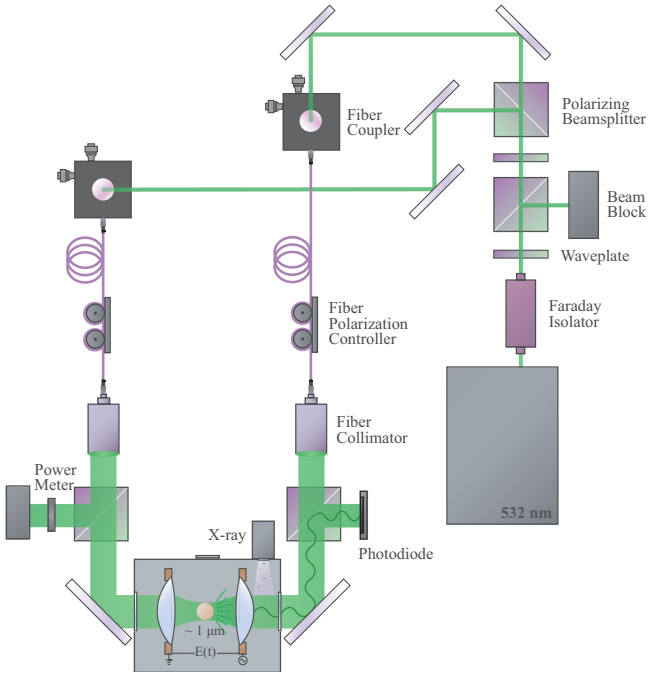

FIG. 1. Experimental setup. The trapping laser (532 nm) is split into two beams by a polarizing beam splitter and coupled into single-mode optical fibers. After being brought back to free space, the beams enter the grounded experimental chamber through one inch windows on either side. Inside, they are focused by two lenses with a focal length of 8 mm to form the trap. Each lens is surrounded by a copper ring electrode. The electric field between these induces oscillations of the particle along the beam axis. We measure the particle's position via changes in the scattered light collected on the photodiode on the right side of the chamber. For particle loading we spray in the aerosol from the port on top of the chamber.

electrodes to apply an electric field along the optical axis. The voltage applied is typically 250 V at frequency $f_{dr} = 2$ kHz, yielding an ac electric field at the particle of $E_0 \approx 8.5 \times 10^3$ V/m.

If the particle is charged, it oscillates at the driving frequency in response to the alternating electric field. Outside the chamber, an inline beam splitter picks off a fraction of the light scattered from the particle and diverts it to a photodiode (Thorlabs, PDAPC2), from which we record continuously at 1 MHz. The measured fluctuations are proportional to the particle's position along the beam axis. We convert this position signal into a real-time charge measurement following the method of Ref. [12]. In brief, this entails comparing the electrically driven contribution to the power spectral density (PSD) of the particle's motion at the driving frequency (S_{el}) to what the PSD would be at the same frequency due to thermal motion alone (S_{th}). The mathematical expression for the particle charge, Q, is

$$Q = \sqrt{\frac{8k_B T\gamma S_{\mathrm{el}}(w_{dr})}{E_0^2 \tau S_{\mathrm{th}}(w_{dr})}}, \tag{1}$$

where k_B, T, and γ are the Boltzmann constant, the temperature, and the drag coefficient, respectively, and τ is the time window over which the PSD is calculated. The full derivation of Eq. (1) can be found in Ref. [12]; for the reader's convenience we provide a sketch in Supplemental Material [21]. To extract the sign of the particle's charge, we additionally monitor the phase of the position oscillations relative to the applied electric field. For computational efficiency, we do not compute the full PSD in every time window but instead use a computational lock-in approach where we measure the charge peak and estimate S_{th}, ignoring other frequency components. S_{el} is measured by computing the squared Fourier component of the raw signal at the driving frequency and subtracting S_{th}, while S_{th} is estimated with the geometric average of the components of the signal ± 300 Hz on either side (far enough from the charge peak so that S_{th} does not change with Q), as illustrated in Fig. 2(a). For these experiments, we used $\tau = 0.2$ s, resulting in five charge measurements per second. To ensure zero particle charge at the beginning of a measurement, we use a soft x-ray source (Hamamatsu L9491) to ionize the air around the particle (without irradiating the particle itself), which enhances the local air conductivity and neutralizes the particle within $\sim 10^{-2}$ s [24]. Figure 2(b) illustrates the decaying oscillations when the x-ray source is switched on, leaving only the particle's Brownian motion in the trap after the discharge is complete. For small Q and low laser intensities, we resolve the particle's electric charge in elementary units, showing every charging (or discharging) event as a discrete step of one elementary charge, $|e|$ [as illustrated for a short duration in Fig. 2(c)].

Figure 3(a) shows the main experimental results, which are charge vs time curves for different powers of the trapping laser. As can be seen, the charging evolution depends on the laser power applied to the optical trap as well as on time. At first, the charging rate is quite linear, but as time progresses, it slows down considerably. In Fig. 3(b), we plot the initial charging rate as a function of the laser intensity, I, with error bars calculated in each case from three independent runs. This data fits precisely to I^2—a clear signature of some kind of two-photon process associated with the charging mechanism. Although the charging rate of each curve slows down over time, data like those shown in Fig. 3 do not fit to typical saturating functions—e.g., a saturating exponential, hyperbolic tangent, or rational function. At very long times, i.e., much longer than the 2200 s shown in Fig. 3, we do encounter an upper limit, but this is due to the fact that the particle becomes so charged that it causes breakdown in the surrounding air—see Supplemental Material [21].

While it is evident from Fig. 3(b) that two-photon absorption is involved in the observed charging, it is not immediately clear how. The valence band maximum of SiO_2 is typically reported to be in the range of ~ 10 eV

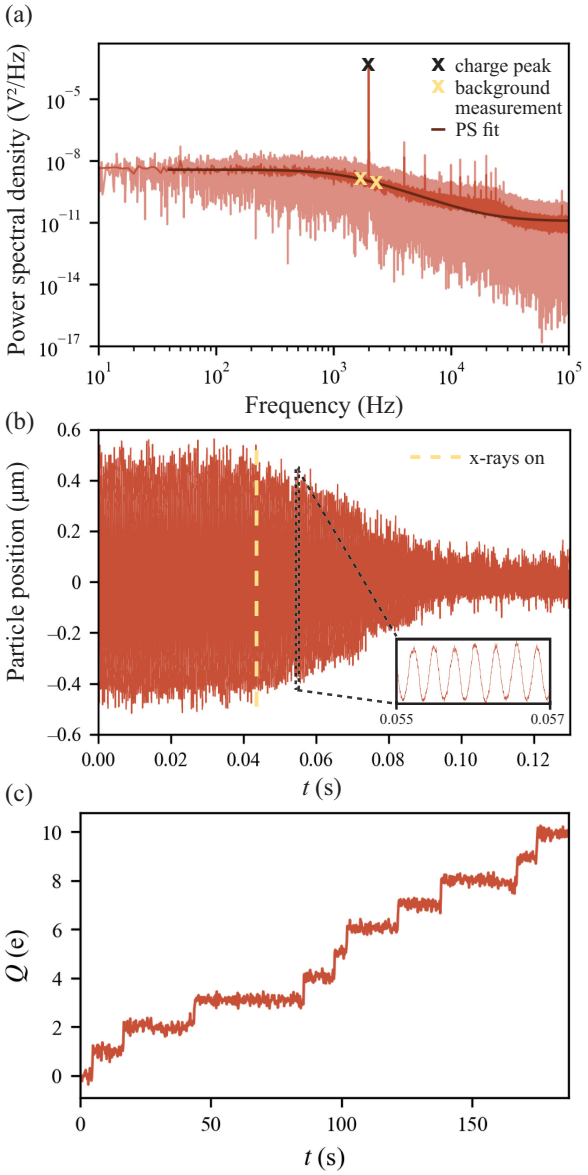

FIG. 2. Measurement principle. (a) The power spectral density (PSD) of the electrically driven particle shows a clear peak at the driving frequency $f_{dr} = 2$ kHz. To obtain the particle's charge, we perform a lock-in style measurement of this charge peak as well as the background PSD values at $f_{dr} \pm 300$ Hz. (b) The particle position oscillates around the trap center with a frequency f_{dr}. After the x-ray source is turned on to discharge the particle, the oscillations decay exponentially. (c) Time evolution of the particle charge showing individual elementary charge steps.

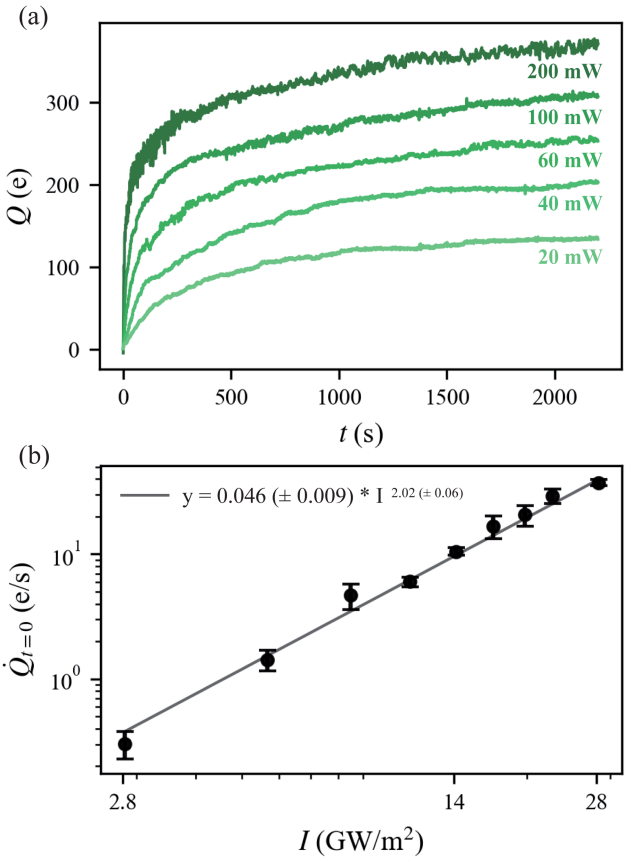

FIG. 3. Charge evolution. (a) First 2200 s of the charging curves of the particle at different laser powers applied to the optical trap. (b) Initial charging rate (up to ~150 e) versus laser intensity I. The square-law dependence shows that the particle is ionized by a two-photon process.

below the vacuum level [25–28]; hence, two of our green photons ($2h\nu \approx 4.66$ eV) are insufficient for direct liberation to air from the valence band. On the other hand, there can be in-gap states in amorphous SiO_2 above the valence band maximum, i.e., arising from structural defects and the disordered nature of the material [29–31]. Assuming that the liberated electrons come from these states, we can imagine two physical interpretations that explain our observations. As it turns out, both result in the same logarithmic fitting equation, which describes our data well. For brevity's sake, we sketch only the essential physics behind these models here; full derivations are in Supplemental Material [21].

In the first interpretation, we suppose that some relevant initial electronic state in the band gap is at an energy below free, ϵ, deeper than $2h\nu$; hence two-photons are insufficient for direct liberation. Even so, if the deficit ($\delta = \epsilon - 2h\nu$) is not too large, it is plausible that two-photon excitation can occur to some intermediate state (e.g., the conduction band), which could then be followed by full liberation via thermal emission. Initially, the barrier to thermal emission would be the energy deficit, δ. However, as the charge of the particle grows, the additional electrostatic barrier, $(Qe/4\pi\epsilon_0 r)$, must be overcome. In the case that the fraction of thermally escaping electrons is small compared to the steady-state population in the intermediate state, it can be shown that this scenario leads to the charging rate equation,

$$\frac{dQ}{dt} \propto I^2 e^{-b_t \frac{Qe}{4\pi\epsilon_0 r k_B T}}, \tag{2}$$

where k_B is Boltzmann's constant, T is temperature, and b_t should be equal to unity (more on this later).

In the second scenario, we imagine that there is a *distribution* of occupied electronic states in the band gap as a function of the energetic depth, ϵ, and that electrons of sufficiently shallow energies in this distribution can be directly liberated via the two-photon process. We define the cumulative distribution of these occupied states, i.e., the total number between 0 and ϵ, as $N(\epsilon)$. If the particle has charge Q, then the total number of electrons that can possibly be liberated is $N[2h\nu - (Qe/4\pi\epsilon_0 r)]$. The inclusion of the Coulombic term now indicates that the two-photon energy must be sufficient to liberate from the material and overcome the electrostatic well of the charged particle. In addition to the I^2 dependence, the charging rate should be proportional to this number. Hence, in this scenario the rate equation is

$$\frac{dQ}{dt} \propto I^2 N\left(2h\nu - \frac{Qe}{4\pi\epsilon_0 r}\right). \tag{3}$$

As can be seen, if the cumulative distribution of intergap states is exponential, i.e., if $N(\epsilon) \propto e^{b_d \epsilon}$ (with b_d an unknown coefficient not necessarily related to $k_B T$), then Eqs. (2) and (3) are functionally identical.

In either case, the differential equation is easily solved, subject to the initial condition $Q(0) = 0$ as enforced by our initial discharge of the sphere. The solution is of the form

$$Q(t) = \frac{4\pi\epsilon_0 r}{Be} \ln\left(\frac{e}{4\pi\epsilon_0 r} ABI^2 t + 1\right). \tag{4}$$

Here, A and B are fitting constants related to the coefficient in front of I^2 and the proportionality factors in the exponential (b_t or b_d, dependent on the model). As we explain in Supplemental Material, care has to be taken regarding the exact definitions of A and B in each case [21]. As we show in Fig. 4(b), this functional form fits our data well, recovering all of the essential features. In particular, we observe that the curves are proportional to I^2 initially and that the charging rate slows down but does not show obvious saturation behavior.

Which physical interpretation is correct? The thermal emission model is appealing in that it offers a first-principles motivation for the exponential in the rate equation (i.e., the Boltzmann factor), yet here is where it also has a significant drawback. As we show in Supplemental Material [21], the b_t parameter extracted for the thermal model is different from unity by about a factor of $\times 10$. This could in principle be consistent with an elevated temperature of the particle; however, due to the low absorption coefficient of silica at

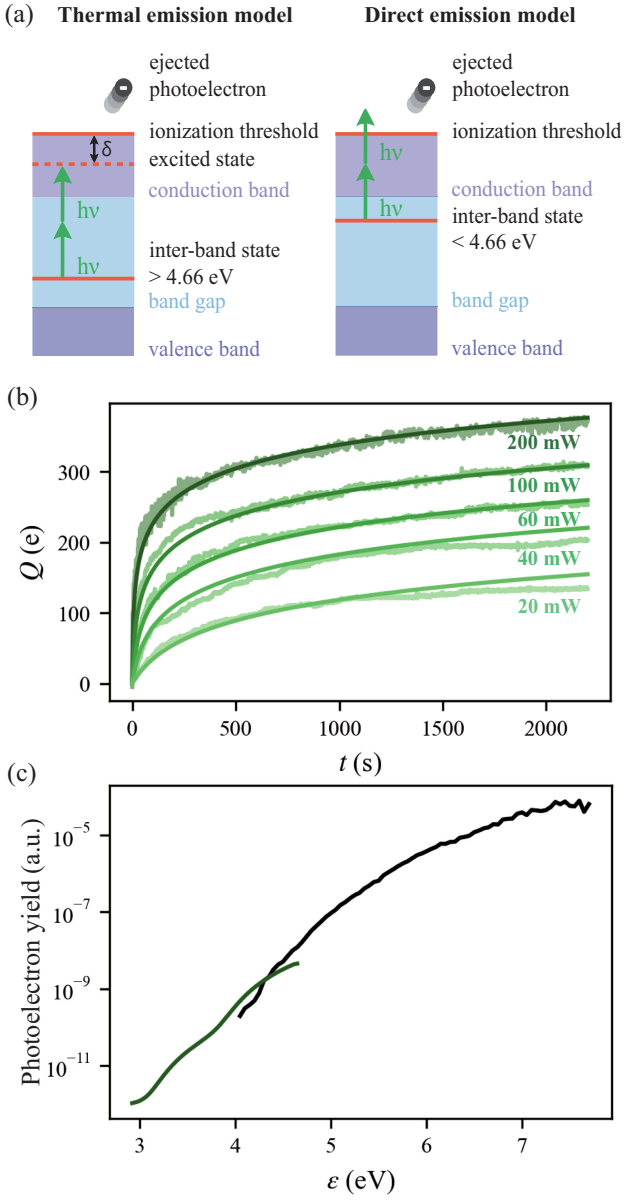

FIG. 4. Illustration of the two proposed models, experimental and modeled charging curves and photoelectron yield spectrum of our sample. (a) In the thermal emission model (left), an electron is excited from a deeper (> 4.66 eV) trap state by the simultaneous absorption of two green photons. From this excited state, the remaining ionization barrier δ is overcome thermally, resulting in the emission of an electron. In the direct emission model (right) the energy of two photons is enough to directly eject an electron from a trap state shallower than 4.66 eV. (b) Experimental data (background) and model charging curves predicted from Eq. (4) (foreground). (c) Photoelectron yield spectroscopy data for our sample in bulk powder form (black). The green curve shows the (rescaled) charging rate versus ionization energy for one of our 200 mW curves from the optical tweezers experiment. The data show the same exponential growth as the PYS data and reveal ionization events at energies as low as 3 eV.

the trapping wavelength, it should remain very close to ambient temperature ~23 °C (see Supplemental Material [21]). On the face of it, the direct-emission model would seem to have the disadvantage that it requires an exponentially distributed population of states in the gap without a first principles motivation. Perhaps ironically, this is where the direct-emission becomes more tenable. In Fig. 4(c), we present photoelectron yield spectroscopy (PYS) data for our samples in bulk powder form. These data were taken on a dedicated PYS-instrument that is independent from our main optical tweezers experiment (see Supplemental Material for details on PYS measurements [21]). In this data, tunable UV light illuminates the sample, and the resulting photocurrent (yield) is measured. The data show that the yield grows exponentially with the single-photon energy, which is consistent with the assumption that the cumulative distribution of states, $N(\epsilon)$, grows exponentially with ϵ. Moreover, while the PYS data are only reliable down to about 4 eV, we can extract an effectively identical yield vs energy curve from our single sphere data in our optical trap [i.e., from the curves in Fig. 3(a)], which reveals that it has the same factor in the exponential (b_d) and extends the range down to as little as 3 eV [green curve in Fig. 4(c); see Supplemental Material for details [21]].

Photoemission curves such as those shown in Fig. 4(c) with broad exponential dependencies in the band gap are routinely observed in amorphous materials and are commonly attributed to the nonequilibrium electronic landscape due to structural disorder [31,32]. The existence of exponential tail states for SiO_2 is also suggested from photoemission measurement in Supplemental Material [21]. Hence, there is precedent to view our data with this picture in mind. Practically, however, we are not able to distinguish between the two physical interpretations using our current optical tweezers setup. We cannot exclude the possibility that the thermal picture is ultimately correct, but some additional ingredient that we are not considering makes the factor b_t different from unity. For instance, the distribution of charges could be spherical due to the presence of the ac electric field, thereby facilitating electron escape. As the thermal emission scenario is sensitive to temperature in a clearly defined way, whereas the direct emission scenario is not, a future direction for experiments could be to incorporate temperature control, e.g., via an additional deep IR laser that, in contrast to our green laser, is significantly absorbed by and can therefore heat the particle. Beyond either of the proposed mechanisms, additional contributions, e.g., lowering of the escape barrier via the Poole–Frenkel effect [33] caused by the applied field, might also be considered. Yet, the present functional form already fits the data quite well.

The simultaneous capacity to levitate a micron-scale (or smaller) particle, measure its charge with electron-scale resolution, and charge it to the maximum amount that it can sustain before dielectric breakdown occurs is significant, offering potential uses across various fields. Our data already show that it offers a way to probe electronic states, creating a retarding potential that is relatively easy to understand and account for. Of special interest to the authors is the potential to study charging dynamics with particles relevant to aerosol and cloud electrification. Understanding how these particles acquire and—perhaps as importantly—*lose* charge (e.g., as demonstrated in Supplemental Material [21]) could provide new insights into some of the most persistent questions in these topics, for instance, lightning initiation. Furthermore, it is easy to envision straightforward additions to the technique that expand its usefulness. Existing experiments with optical tweezers already show that lower energy photons (e.g., in the near IR [8,9,12]) generally avoid the charging mechanism that we observe; hence by overlapping one "trapping" laser (near IR) and one "charging" laser (such as ours), a particle's charge could be brought to a desired value and then "set free" to evolve in different environmental conditions. Moreover, with a sufficiently high energy UV laser, the charging mechanism need not be from a two-photon process, and as we suggested earlier an overlapping deep IR laser could be used to heat the particle to enable temperature-dependent studies. These possibilities position optically levitated particles as a unique platform for probing complex, charge-related behavior of microscopic particles across a wide range of disciplines, with a level of control, specificity, and resolution that is difficult to achieve by other means.

Acknowledgments—We thank Todor Asenov and Abdulhamid Baghdadi for their outstanding technical support and Dr. Michael Gleichweit and Mercede Azizbaig Mohajer for the helpful discussions. This project has received funding from the European Research Council (ERC) under the European Union's Horizon 2020 research and innovation programme (Grant Agreements No. 949120 and No. 805041) and the Swiss National Science Foundation (SNSF, Project No. 200021-236446). This research was supported by the Scientific Service Units of the Institute of Science and Technology Austria (ISTA) through resources provided by the Miba Machine Shop and the Scientific Computing service unit.

Data availability—The data that support the findings of this article are not publicly available upon publication because it is not technically feasible and/or the cost of preparing, depositing, and hosting the data would be prohibitive within the terms of this research project. The data are available from the authors upon reasonable request.

[1] J. W. Merrill, S. K. Sainis, and E. R. Dufresne, Phys. Rev. Lett. **103**, 138301 (2009).
[2] L. Mitchem and J. P. Reid, Chem. Soc. Rev. **37**, 756 (2008).

[3] M. A. Mohajer, P. Basuri, A. Evdokimov, G. David, D. Zindel, E. Miliordos, and R. Signorell, Science **388**, 1426 (2025).
[4] R. C. Sullivan, H. Boyer-Chelmo, K. Gorkowski, and H. Beydoun, Acc. Chem. Res. **53**, 2498 (2020).
[5] D. B. Ruffner and D. G. Grier, Phys. Rev. Lett. **108**, 173602 (2012).
[6] H. Rubinsztein-Dunlop, A. B. Stilgoe, D. Preece, A. Bui, and T. A. Nieminen, in *Photonics* (John Wiley & Sons, Inc., Hoboken, NJ, USA, 2015), pp. 287–339, 10.1002/9781119011781.ch7.
[7] R. A. Millikan, Phys. Rev. **2**, 109 (1913).
[8] F. Beunis, F. Strubbe, B. Verboven, K. Neyts, and D. Petrov, Proc. SPIE **7613**, 1 (2009)..
[9] F. Beunis, F. Strubbe, K. Neyts, and D. Petrov, Phys. Rev. Lett. **108**, 016101 (2012).
[10] C. Schreuer, S. Vandewiele, F. Strubbe, K. Neyts, and F. Beunis, J. Colloid Interface Sci. **515**, 248 (2018).
[11] C. Schreuer, S. Vandewiele, T. Brans, F. Strubbe, K. Neyts, and F. Beunis, J. Appl. Phys. **123**, 015105 (2018).
[12] F. Ricci, M. T. Cuairan, G. P. Conangla, A. W. Schell, and R. Quidant, Nano Lett. **19**, 6711 (2019).
[13] S. Zhu, Z. Fu, X. Gao, C. Li, Z. Chen, Y. Wang, X. Chen, and H. Hu, Photonics Res. **11**, 279 (2023).
[14] G. Pesce, G. Rusciano, G. Zito, and A. Sasso, Opt. Express **23**, 9363 (2015).
[15] M. Frimmer, K. Luszcz, S. Ferreiro, V. Jain, E. Hebestreit, and L. Novotny, Phys. Rev. A **95**, 061801 (2017).
[16] J. T. Marmolejo, M. Urquiza-González, O. Isaksson, A. Johansson, R. Méndez-Fragoso, and D. Hanstorp, Sci. Rep. **11**, 10703 (2021).
[17] F. Ricci, M. T. Cuairan, A. W. Schell, E. Hebestreit, R. A. Rica, N. Meyer, and R. Quidant, ACS Nano **16**, 8677 (2022).
[18] J. Wang, C. Li, S. Zhu, C. He, Z. Fu, X. Zhu, Z. Chen, and H. Hu, Appl. Phys. Express **16**, 066502 (2023).
[19] A. Ashkin and J. M. Dziedzic, Phys. Rev. Lett. **36**, 267 (1976).
[20] O. Reich, M. J. Gleichweit, G. David, N. Leemann, and R. Signorell, Environ. Sci. Atmos. **3**, 695 (2023).
[21] See Supplemental Material at http://link.aps.org/supplemental/10.1103/5xd9-4tjj for details on sample preparation, charge measurement, photoelectron yield spectroscopy, charging models, and additional data, which includes Refs. [22,23].
[22] D. Petersen, M. Bailey, J. Hallett, and W. Beasley, Q. J. R. Meteorol. Soc. **141**, 1283 (2014).
[23] J. Bateman, S. Nimmrichter, K. Hornberger, and H. Ulbricht, Nat. Commun. **5**, 4788 (2014).
[24] W. C. Hinds, *Aerosol Technology: Properties, Behavior, and Measurement of Airborne Particles* (John Wiley & Sons, Incorporated, New York, 1999).
[25] H. Ishii, S. Masuda, and Y. Harada, Surf. Sci. **239**, 222 (1990).
[26] N. Fujimura, A. Ohta, K. Makihara, and S. Miyazaki, Jpn. J. Appl. Phys. **55**, 08P (2016).
[27] M. L. O'Brien, C. Koitzsch, and R. J. Nemanich, J. Vac. Sci. Technol. B Microelectron. Nanometer Struct. Process. Meas. Phenom. **18**, 1776 (2000).
[28] C. C. Fulton, G. Lucovsky, and R. J. Nemanich, J. Appl. Phys. **99**, 063708 (2006).
[29] V. Astašauskas, A. Bellissimo, P. Kuksa, C. Tomastik, H. Kalbe, and W. S. M. Werner, J. Electron Spectrosc. Relat. Phenom. **241**, 146829 (2020).
[30] D. L. Griscom, J. Non Cryst. Solids **73**, 51 (1985).
[31] J. F. Wager, AIP Adv. **7**, 125321 (2017).
[32] J. Singh and K. Shimakawa, *Advances in Amorphous Semiconductors* (Taylor & Francis, London, 2003).
[33] J. Frenkel, Phys. Rev. **54**, 647 (1938).